The Journal of Physical Chemistry Letters

Letter

Cite This: J. Phys. Chem. Lett. 2018, 9, 1534−1541

pubs.acs.org/JPCL

UV-Light-Induced Vibrational Coherences: The Key to Understand Kasha Rule Violation in *trans*-Azobenzene

Artur Nenov,[†,○] Rocio Borrego-Varillas,[‡,○] Aurelio Oriana,[‡,◆] Lucia Ganzer,[‡] Francesco Segatta,[†,⊥] Irene Conti,[†] Javier Segarra-Marti,[§] Junko Omachi,[∥] Maurizio Dapor,[⊥] Simone Taioli,[⊥,#] Cristian Manzoni,[‡] Shaul Mukamel,[∇] Giulio Cerullo,[*,‡] and Marco Garavelli[*,†]

[†]Dipartimento di Chimica Industriale, Università degli Studi di Bologna, Viale del Risorgimento 4, I-40136 Bologna, Italy

[‡]IFN-CNR, Dipartimento di Fisica, Politecnico di Milano, Piazza Leonardo da Vinci 32, I-20133 Milano, Italy

[§]Laboratoire de Chimie UMR 5182, Université Lyon, ENS de Lyon, CNRS, Université Lyon 1, 46 Allée d'Italie, FR-69342 Lyon, France

[∥]Institute for Photon Science and Technology, University of Tokyo, 7-3-1 Hongo, Bunkyo-ku, Tokyo 113-0033, Japan

[⊥]European Center for Theoretical Studies in Nuclear Physics and Related Areas (ECT*-FBK) and Trento Institute for Fundamental Physics and Applications (TIFPA-INFN), 38123 Trento, Italy

[#]Faculty of Mathematics and Physics, Charles University, Praha 8, 180 00 Prague, Czech Republic

[∇]Department of Chemistry, University of California, Irvine, California 92697-2025, United States

Supporting Information

ABSTRACT: We combine sub-20 fs transient absorption spectroscopy with state-of-the-art computations to study the ultrafast photoinduced dynamics of *trans*-azobenzene (AB). We are able to resolve the lifetime of the $\pi\pi^*$ state, whose decay within ca. 50 fs is correlated to the buildup of the $n\pi^*$ population and to the emergence of coherences in the dynamics, to date unobserved. Nonlinear spectroscopy simulations call for the CNN in-plane bendings as the active modes in the subps photoinduced coherent dynamics out of the $\pi\pi^*$ state. Radiative to kinetic energy transfer into these modes drives the system to a high-energy planar $n\pi^*$/ground state conical intersection, inaccessible upon direct excitation of the $n\pi^*$ state, that triggers an ultrafast (0.45 ps) nonproductive decay of the $n\pi^*$ state and is thus responsible for the observed Kasha rule violation in UV excited *trans*-AB. On the other hand, cis-AB is built only after intramolecular vibrational energy redistribution and population of the NN torsional mode.

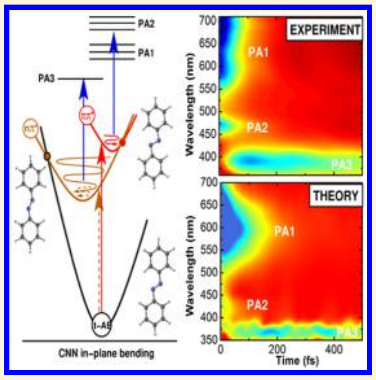

Photochromism is at the heart of light-powered nanomachines, also known as molecular photoswitches, which can be reversibly switched between two or more stable configurations by exposure to light.[1] Over the years, the technological potential of molecular switches has been demonstrated in various applications like optical storage devices,[2] triggers for peptide folding,[3,4] light-gated ion channel control[5] or nonlinear optical materials[6] to name a few. Azobenzene (AB) based compounds are prominent photoswitches that undergo an ultrafast (picosecond) *trans*−*cis* photoisomerization associated with changing the conformation of the central N═N double bond. AB has favorable photochromic properties, such as a significant change in geometry of the molecule upon isomerization, photoactivity even under strong constraints,[7−11] and discrete absorption bands, allowing one to selectively address either the *trans* or *cis* configurations. It is therefore not surprising that considerable effort has been put into scrutinizing its photoactivity.[8,12−39] A summary of the most notable research is provided in section 8 of the Supporting Information (SI). Nowadays it is generally accepted that the decay to the ground state (GS) upon $n\pi^*$ excitation of *trans*-AB involves an extended conical intersection (CI) seam reached through both torsion and bending ("inversion-assisted torsion", Scheme 1b). However, there is still a controversy over key aspects of the photoisomerization process of $\pi\pi^*$-excited *trans*-AB. To date, the temporal resolution of transient experiments has not permitted one to determine the lifetime of the $\pi\pi^*$ state ($?_1$ in Scheme 1a). To the best of our knowledge a value of 110 fs[25] is the shortest lifetime reported in the literature, which is comparable to the used instrumental response function (see Scheme 1c for a literature survey of $\pi\pi^*$ and $n\pi^*$ lifetimes after $\pi\pi^*$ excitation). Following the ultrafast decay of the spectral features associated with the $\pi\pi^*$ state a biexponential (subpicoseconds and several picoseconds) decay of the $n\pi^*$-associated signatures has been reported. While there is strong evidence for a pathway common to $\pi\pi^*$- and $n\pi^*$-excitation[18,20,25,26] (i.e., inversion-assisted torsion, shown in blue and red in Scheme 1a), it is still unclear

Received: January 16, 2018
Accepted: March 5, 2018
Published: March 5, 2018

DOI: 10.1021/acs.jpclett.8b00152
J. Phys. Chem. Lett. 2018, 9, 1534−1541

Scheme 1. (a) Energy Diagrams of the Relaxation Channels in *trans*-AB after nπ^*- and $\pi\pi^*$- Excitation, Proposed in the Literature; (b) The *trans* → *cis* Mechanism of Inversion-Assisted Torsion; (c) Literature Survey of the of $\pi\pi^*$ and nπ^* Lifetimes after $\pi\pi^*$ Excitation

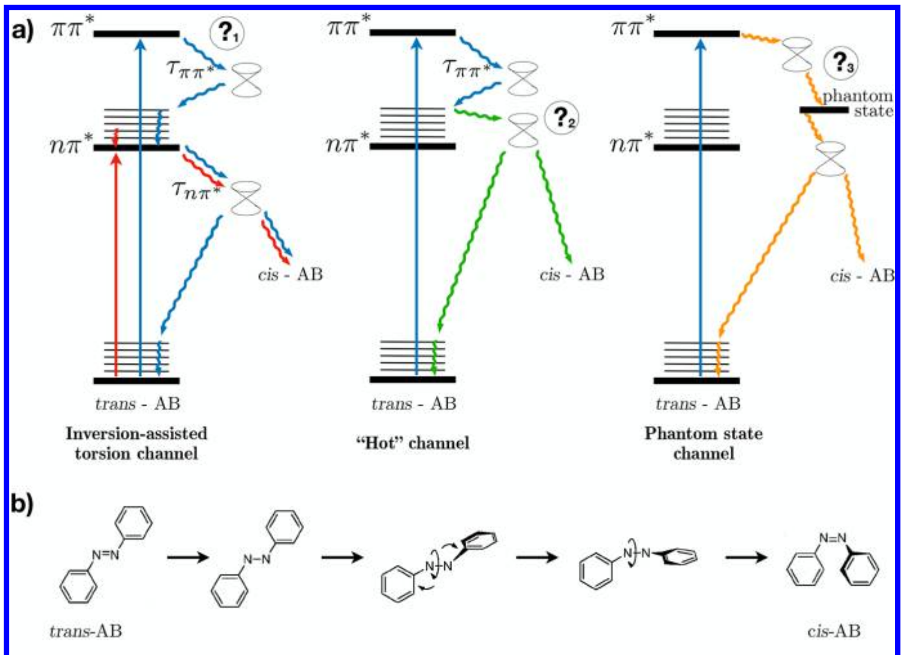

c)

Solvent	Pump λ (nm)	$\tau_{\pi\pi^*}$ (fs)	$\tau_{n\pi^*}$ (ps)	Time resolution (fs)	Ref.
hexane	267	< 500	0.94 & 16.9	600	17
	280		0.8 & 14	180	14
	300	< 180	0.8 & 10	180	14
	347	< 180	0.8 & 10	180	14
ethanol	266	130	0.42 & 2.9	200	18
	340	130	0.43 & 2.7	200	18
acetonitrile	300		1.2	200	13
	310	110	0.37 & 2.3	100	25

what is the nature of the molecular motion associated with the subps relaxation dynamics. It is speculated that this ultrafast channel involves a CI inaccessible upon nπ^* excitation[25,29] (labeled the "hot" channel in Scheme 1a), but it is yet to be demonstrated whether this relaxation channel is reactive (i.e., leading to *cis*-AB) or nonreactive and whether it is responsible for the violation of the Kasha rule,[8] characterized by a 50% decrease of the quantum yield (QY) upon excitation of *trans*-AB with UV light ($?_2$ in Scheme 1a). Related to this, the involvement of "dark" states (labeled the "phantom" state in Scheme 1a), brought into discussion by several authors[21,28,33] as a possible reason for the QY decrease, still remains controversial ($?_3$ in Scheme 1a).

In this paper, we address these questions by combining high time resolution transient absorption (TA) spectroscopy and multiconfigurational wave function techniques. We perform TA with sub-20 fs pump pulses at 320 nm and broadband probe pulses ranging from the visible (350–700 nm) to the UV (250–380 nm), which (a) allow one to resolve the dynamics in the $\pi\pi^*$ state prior to its ultrafast (sub-100 fs) decay, (b) resolve coherent ES dynamics in the nπ^* state, and (c) explore the deep UV window (250–280 nm) rich with spectroscopic fingerprints of reactant and photoproduct. *Ab initio* molecular dynamics (MD) simulations within the second-order multiconfigurational perturbation theory (CASPT2) framework utilizing a full-π active space disclose the relaxation routes from the Franck–Condon (FC) point on the $\pi\pi^*$ state to the GS, thereby confirming the ultrafast $\pi\pi^* \rightarrow n\pi^*$ decay. The simulations show that the "hot" nπ^* population can decay to the GS through an energetically high lying near-planar region of the nπ^*/GS CI seam not accessible upon selective excitation of the nπ^* state, thus confirming the existence of the "hot" decay channel (Figure 1a). We argue that this channel is nonreactive and, thus, the prime reason for the violation of the Kasha rule. Combining high-level electronic structure calculations with theoretical nonlinear spectroscopy techniques, we simulate the TA spectra, explicitly incorporating the, so far, theoretically elusive excited state absorption (ESA) features and their vibrational line shape broadening, therefore uncovering the nature of the coherent oscillations observed in the experiment.

Trans-AB in ethanol solution was pumped with 16 fs UV pulses centered at 330 nm, resonant with the $\pi\pi^*$ transition, and probed over a broad wavelength range. The experimental setup has been described elsewhere,[40−42] whereas the sample preparation details and the linear absorption (LA) spectrum are provided in the SI. Figure 1(a) shows the TA spectra in the visible (VIS) between 360 and 700 nm for the first 500 fs. In agreement with previous studies,[14,17,18,25] at early times (<100 fs) we observe two photoinduced absorption (PA) bands: a broad intense band ranging from 550 to 700 nm (PA1) and a narrower band between 450 and 500 nm (PA2). A global fit of the data[49,50](see SI for details) reveals that PA1 and PA2 decay

DOI: 10.1021/acs.jpclett.8b00152
J. Phys. Chem. Lett. 2018, 9, 1534−1541

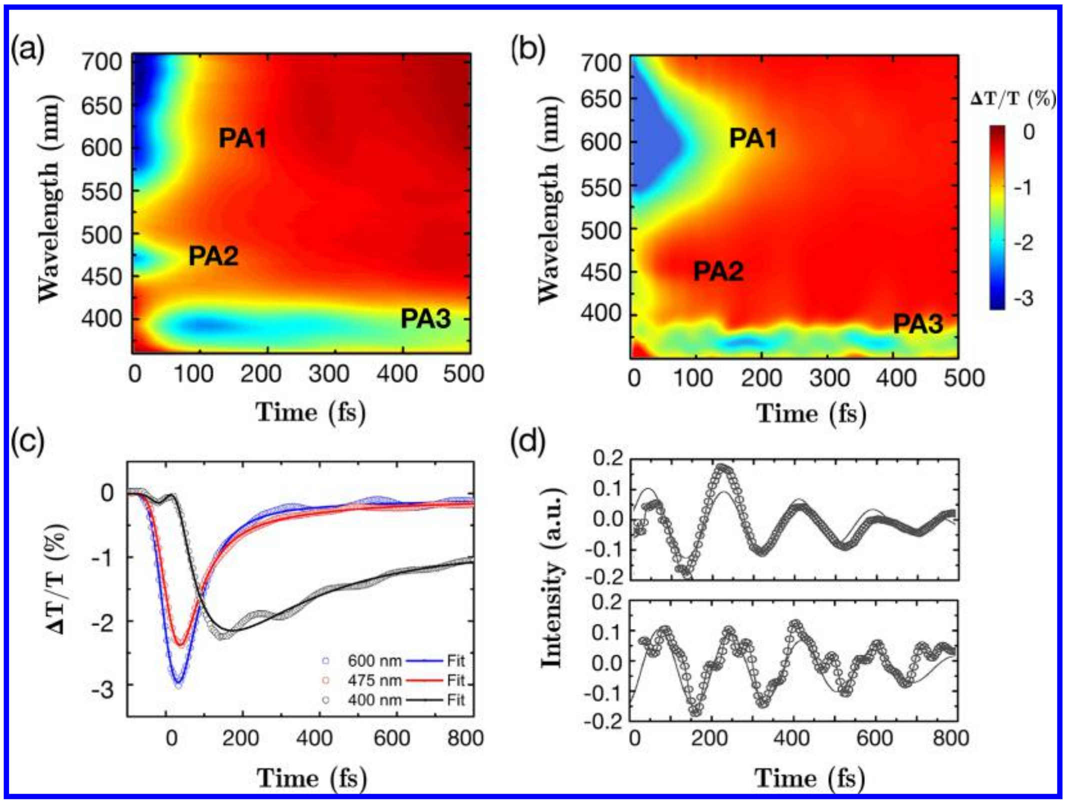

Figure 1. (a) Experimental (ethanol) and (b) theoretical (gas-phase) TA maps of *trans*-AB in the visible spectral window during the first 500 fs with (c) extracted dynamics at 400, 475, and 600 nm. (d) Intensity oscillations (residuals): experimental at 400 nm (top) and computed at 370 nm (bottom). Open dots represent the experimental (theoretical) data, and the solid line the fits.

with a lifetime of ~50 fs (Figure 1c), with the concurrent rising of a new PA band (PA3), formed with the same time constant, peaking around 400 nm. Considering their ultrafast decay and their absence in the spectra when the nπ* state is selectively excited, PA1 and PA2 have been previously assigned to the $\pi\pi$* state.[18,25,26] PA3, on the other hand, is a fingerprint of the nπ* state.[18−20,25,26] It shows oscillatory behavior with a period of 170 fs (195 cm^{-1}), an indication of coherent dynamics, damped after ≈2 ps. Similar oscillatory patterns are observed also at 600 and 670 nm, after the initial fast amplitude decay. Measurements on longer time scale (Figures S20 and S21, SI) show a PA3 decay described by the sum of three exponentials with time constants 0.45 ps, 2.5 ps and ~9 ps, in agreement with previous studies.[18−20,25]

Figure 1b depicts the simulated TA map in the same temporal and spectral windows. The simulations protocol utilizes nonlinear response theory, the system's response to the perturbation by three external electric fields is expressed within the framework of cumulant expansion of Gaussian fluctuations (CGF)[43−45] and the parameters were obtained with electronic structure computations within the framework of multiconfigurational wave function theory.[46−48] The simulation protocol is outlined in Sections 1 and 2 of the SI. Despite the notable blue-shift of the computed signals with respect to experiment (that falls within the accuracy of the computational approach) the agreement is excellent. These results allow us to identify the nature of the underlying transitions. The rapidly decaying PA1 and PA2 features are fingerprints of the $\pi\pi$* state, which arise due to the spectral overlap of ESA bands associated with several electronic transitions. Each of the two ESA signals consists of three higher lying states which are bright from the $\pi\pi$* state and have a pronounced multiconfigurational nature and significant weights of doubly excited configuration state functions (SI, PA1: section 3.2.2, Figure S12 and Table S5).

ESA bands provide an indirect probe of the coherent vibrational dynamics in the ES reflected in peak shifts and intensity beats, whose magnitude is correlated to the electronic structure of the underlying states. The states contributing to PA1 and PA2 show pronounced sensitivity to the following ES-active modes: 606/614 cm^{-1}, 666 cm^{-1}, 924 cm^{-1}, 1161 cm^{-1}, 1397 and 1628 cm^{-1}, associated with bending and stretching deformations in the central CNNC fragment (Figures S5 and S6 in the SI). The ultrafast decay of the population covers coherent oscillatory features at early times. The picture is clearer when looking at the 400 nm trace (Figure 1c), the fingerprint of the nπ* state. It arises from a single ESA contribution to a higher lying state (SI, section 3.2.3 and Table S6). As noted above, the intensity of PA3 shows clear oscillatory behavior with a 170 fs period. Our simulations (Figure 1d) reproduce the intensity beat pattern rather well. Remarkably, only one dominant vibrational feature (195 cm^{-1}) is extracted from both the experiment and simulation despite the fact that time-resolved Raman[17] and photoionization[31] spectroscopies have resolved a plethora of modes involved in the coherent dynamics on the nπ* state after selective nπ* excitation. Oddly enough, although the CASSCF frequencies at the nπ* minimum provide a 205 cm^{-1} mode (symmetric CNN bending) that could be tentatively assigned to the experimental observation, our simulations demonstrate that the ES responsible for PA3 is rather insensitive to the dynamics in this mode (Figure S8, SI). Instead, our simulations show that

DOI: 10.1021/acs.jpclett.8b00152
J. Phys. Chem. Lett. 2018, 9, 1534−1541

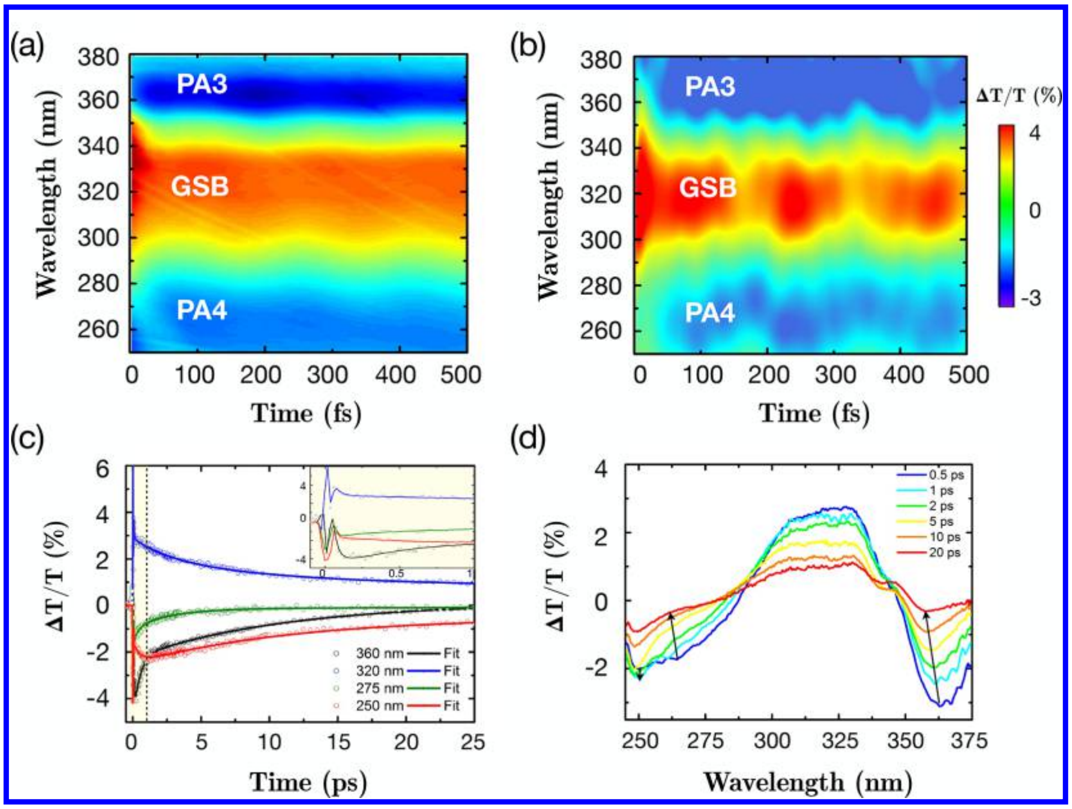

Figure 2. (a) Experimental (ethanol) and (b) theoretical (gas-phase) TA data of *trans*-AB probed in the ultraviolet range (245−380 nm). (c) Experimental dynamics at three selected wavelengths (open circles) and fit of the data (solid lines). Inset: Zoom up to 1 ps delay time. (d) Experimental transient spectra at several delay times. Arrows highlight the blue-shift of the maxima of the transient absorption signals around 270 and 360 nm, and the increase of the signal at 250 nm.

the 660 and 852 cm^{-1} modes, both having strong CNN bending contribution, strongly modulate the absorption cross-section of the ES, and are the source of the observed intensity beats (see Chapter 3.2 in the SI). These frequencies have been reported to be particularly intense in time-resolved Raman studies[15,25] and in photoionization spectroscopy.[31] Together with the 205 cm^{-1} CNN bending and the 300 cm^{-1} CCN bending modes, they constitute a quartet of "hot" modes that accumulate almost 10000 cm^{-1} reorganization energy upon $\pi\pi^* \rightarrow n\pi^*$ decay. We also note a second nπ^* fingerprint PA signal around 600 nm which has been reported previously for selective nπ^* excitation.[18,25] Weak coherent oscillations are resolved in the ps-range. For this ESA, three modes, 205, 660, and 852 cm^{-1}, are predicted to contribute (Figure S13 in the SI).

A second set of measurements was performed with UV (250−380 nm) probe. Figure 2a shows the TA map during the first 500 fs compared to the theory (panel b). A longer time scale measurement is given in the SI (Figures S20 and S21). In addition to PA3, two new spectral features are observed: the GSB in the range 300−340 nm, which decays with a time constant of 11 ps (Figure 2c) and a PA band ranging from 245 to 280 nm (PA4). Global analysis of the spectral features around PA4 reveals 0.46, 2.8, and 11 ps time constants. These values match those of PA3, indicating that the nature of PA4 and PA3 must be similar. This notion is supported by the computations, which also resolve this ESA feature of the nπ^* state (Figure 2b and SI, section 2.2.3 and Table S6). There is, however, one noticeable difference between PA3 and PA4: by comparing the TA spectra (Figure 2d), one observes that while the signals at 365 and 270 nm decrease in amplitude during the first 2 ps accompanied by a blue-shift, PA4 shows a simultaneous increase in amplitude at the bluest frequencies (245−260 nm) on the same time scale. At longer delay times, the entire band relaxes with a lifetime of 11 ps, leaving a finite long-lived offset due to the formed *cis*-AB. Correspondingly, a fit of the signal at 250 nm shows a build-up time of 0.46 ps, and decay constant of 11 ps. A global analysis of the data (SI, Figure S23) reveals that the bluest region (245−260 nm) is dominated by the 0.46 and 11 ps components, whereas in the reddest region (260−280 nm) the 0.46 and 2.8 ps components present the largest amplitude. Thus, these two spectral regions of PA4 capture different processes whose signatures overlap spectrally and temporally. The LA spectrum of *cis*-AB (see Figure 1 in ref 25) shows a peak at 250 nm. Thus, one might tentatively assign the buildup of intensity at this wavelength to the formation of *cis*-AB in the GS on a subpicosecond time scale. However, we argue that we observe more probably a signature of the "hot" *trans*-AB reactant. Kovalenko et al. estimated that ≈50% of the nπ^* population returns to the GS within the first ps. Even if we assumed that all of the *cis*-AB photoproduct (∼12% QY) is formed through this ultrafast channel, at least four times more "hot" reactant would be recovered simultaneously. It is well-known that a "hot" GS gives rise to a PA band red-shifted from the GSB, which decays by vibrational cooling on a picosecond time scale. The LA spectrum of *trans*-AB has a narrow band peaking at ≈230 nm, assigned by our computations to a transfer of electronic density between the central CNNC fragment and the benzene rings (SI, Table S4). Thus, we interpret the 250 nm signal as the buildup of the "hot" GS of

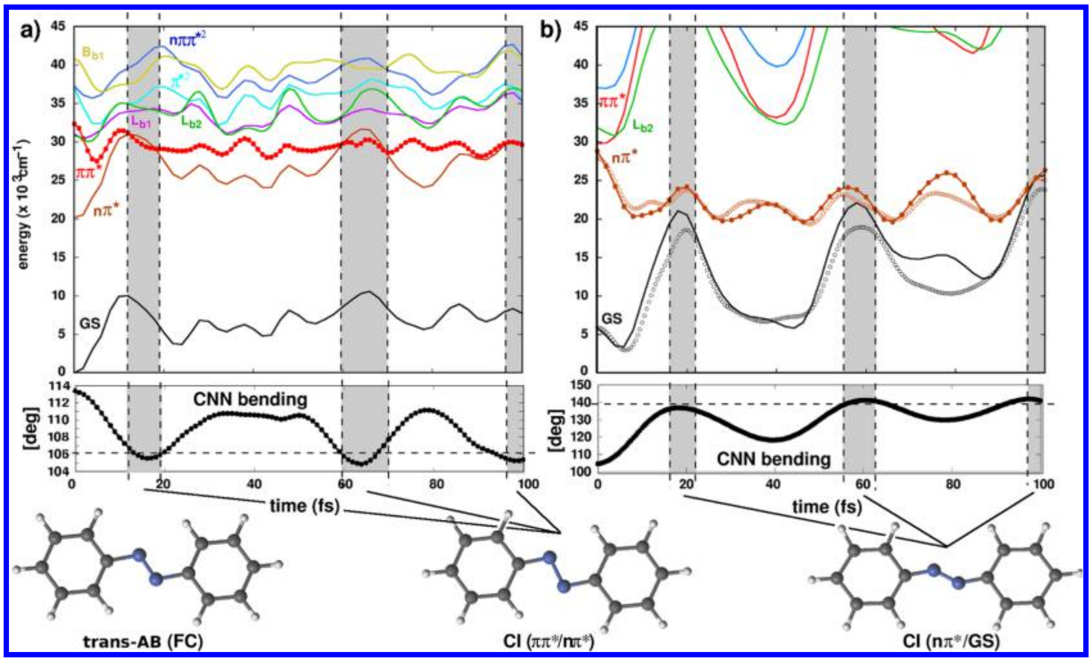

Figure 3. Structure of the low-lying ES manifold along the 0 K MD in the $\pi\pi^*$ state (red) initiated at the FC point (a) and along the nπ^* state (brown) initiated at a CI between $\pi\pi^*$ and nπ^* (b). Both symmetry-constrained (solid lines) and fully unconstrained (dashed lines) simulations were performed starting from a planar and a nonplanar CI geometry, respectively. The evolution of CNN bending along the symmetry-constrained trajectories is shown. Gray areas indicate recurrent crossings between $\pi\pi^*$ and nπ^* (a), as well as between nπ^* and GS.

the reactant, whose PA overlaps with the 270 nm ESA of the nπ^* state.

To validate this interpretation and explain the molecular motions governing the ultrafast (subpicoseconds) decay of a major part of the ES population, we performed adiabatic *ab initio* MD simulations utilizing quantum mechanical gradients at CASPT2 level of theory[51] (Figure 3). A single trajectory was initiated in the FC point (C_{2h} symmetry) of the bright $\pi\pi^*$ state (red dotted line in Figure 3a) without initial kinetic energy, and the energies of the close lying electronic states were monitored for the first 100 fs (further details on the simulation protocol are provided in section 4 of the SI). We found a high density of electronic states in the near- and deep-UV energy window (250−400 nm). Two spectroscopically "dark" states involving the benzene rings (purple, Lb1, and green, Lb2, SI, Table S4) appear near isoenergetic with the $\pi\pi^*$ state in the FC point. Further states involve the doubly excited π^{*2} (cyan), the mixed n$\pi\pi^{*2}$ transition (blue) and the aforementioned "bright" state responsible for the 230 nm band in the LA spectrum (Bb1, shown in dark ocher, SI, Table S4). The picture is completed by the nπ^* state at ∼500 nm, the lowest ES in *trans*-AB. In agreement with Raman data,[15,23,31] the vibrational dynamics in the $\pi\pi^*$ state is governed by the N = N and C−N stretching modes with 1397 and 1618 cm^{-1} frequencies. It is apparent that the $\pi\pi^*$ state crosses several times with the nπ^* state, which exhibits a pronounced destabilization in intervals of ca. 40 fs. These recurrent crossings (gray areas in Figure 3a) are correlated to the in-plane CNN bending. We clarify, however, that the $\pi\pi^* \rightarrow$ nπ^* population transfer is symmetry-forbidden for planar geometries. Out-of-plane deformations are required to invoke a nonzero nonadiabatic coupling. Upon releasing the symmetry constrains, we optimized a nonplanar asymmetric CI (SI, section 2.2.3) with a CNNC dihedral of 13°. It is, thus, evident that an extended nonplanar $\pi\pi^*$/nπ^* CI seam is available to *trans*-AB. The need to undergo out-of-plane deformations for efficient population transfer might explain the mismatch between the experimental $\pi\pi^*$ lifetime of 52 fs and the theoretical simulation revealing a crossing as early as 15 fs.

The "dark" benzenic[17] and the doubly excited π^{*2} states have been suggested to participate in the deactivation of the $\pi\pi^*$ state[28,33] ("phantom" states). The best candidate for a potential population bifurcation is one of the benzenic states Lb2 (green line in Figure 3a) due to its energetic proximity to the $\pi\pi^*$ state and to the finite (symmetry-allowed) probability for non-adiabatic population transfer even for planar geometries. However, our simulations show that this state remains above the $\pi\pi^*$ state throughout the dynamics, suggesting that the direct $\pi\pi^* \rightarrow$ nπ^* decay is the most efficient channel, in agreement with our high time resolution TA results. We emphasize that the 0K simulations do not disprove the participation of "phantom" states but merely show that the latter are not necessary to rationalize the spectroscopic features of the present study.

Starting from the nonplanar CI geometry, we followed the molecular dynamics in the nπ^* state through a fully unconstrained simulation for 200 fs (dashed lines in Figure 3b). We chose the nonplanar geometry as a starting point of the simulation to address potential activation of either the (asymmetric) inversion or the torsion mechanism at early times. MD simulations were also performed under C_{2h} symmetry (solid lines in Figure 3b) starting from a planar $\pi\pi^*$/nπ^* CI. The nπ^* exhibits a pronounced destabilization in the $\pi\pi^*$/nπ^* CI region, due to the far out-of-equilibrium displacement along the CNN coordinate with a value of 127° in the nπ^* equilibrium. After crossing to the nπ^* state the wavepacket converts upon relaxation nearly 10000 cm^{-1} potential energy, stored in the CNN bending modes, to kinetic energy. Despite the unconstrained approach, we observe only in-plane dynamics during the first 200 fs governed by the same

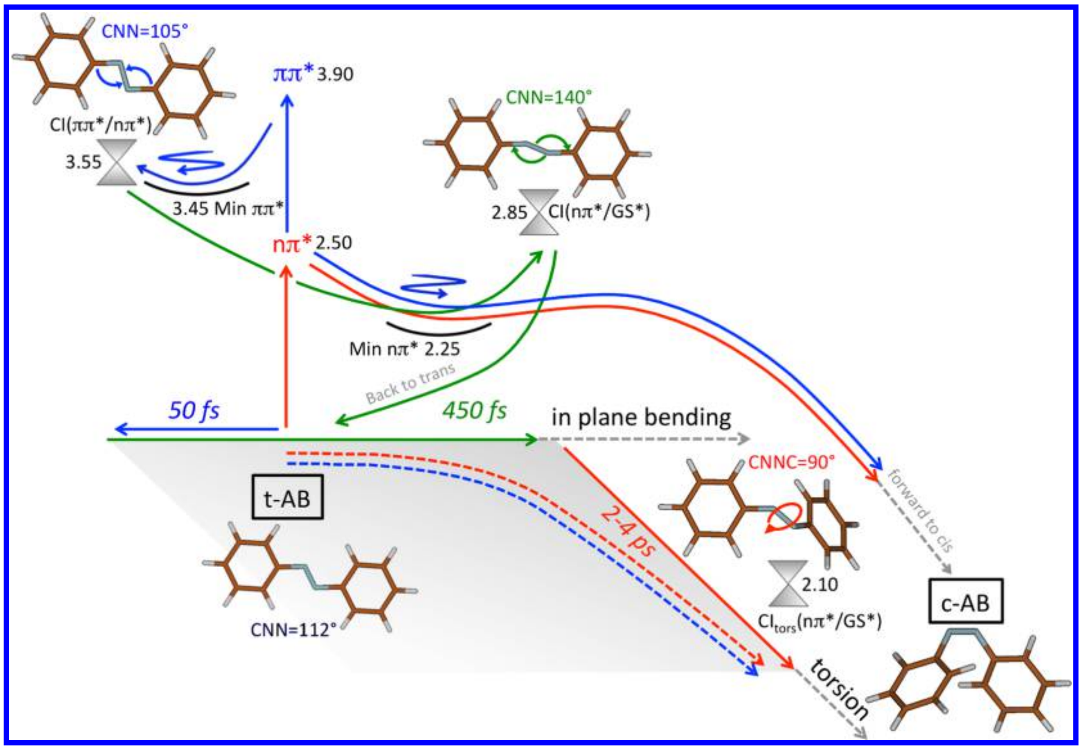

Figure 4. Overview of the photochemistry of trans-AB in the space of the CNN in-plane bending and CNNC torsion modes. Excitation of the bright $\pi\pi^*$ transition in the UV (320 nm) opens a subps nonreactive decay channel to the GS via $\pi\pi^* \rightarrow$ CI($\pi\pi^*$/nπ^*) → nπ^* → CI(nπ^*/GS) ("hot" channel in Scheme 1a). The coherent dynamics associated with this nonreactive channel driven by the in-plane CNN bending mode is the source of ESA intensity beats in the transient spectra and reduced QY. *trans* → *cis* isomerization requires IVR into the torsional mode, takes an order of magnitude longer (2−4 ps), is incoherent, and proceeds in an analogous way upon UV and VIS excitation (500 nm, nπ^* excitation). Dashed lines show projection in the bending-torsion plane. Coloring according to Scheme 1a. Energy values in eV.

four "hot" CNN modes responsible for the intensity beat pattern observed in the VIS spectra. In fact, the unconstrained dynamics follows closely the dynamics within C_{2h} symmetry. The vibrational energy inserted in the bending modes drives AB within 20 fs away from the $\pi\pi^*$/nπ^* CI far beyond the nπ^* equilibrium toward a CI with the GS situated ~5000 cm^{-1} above the nπ^* minimum and showing an increase of the CNN angles to 143°.[29] The CI region is revisited every 40 fs. It is this energetically high lying segment of the CI seam with nearly planar geometries, which remains inaccessible after direct nπ^* excitation, that effectively funnels half of the nπ^* population back to the GS within the first 500 fs after $\pi\pi^*$ excitation. We argue that this channel should be essentially nonreactive because (a) we do not observe the activation of asymmetric bending modes required to reach *cis*-AB, (b) a finite barrier exists in the GS along the 143° → 180 °CNN increase required to reach the transition state region, and (c) the crossing seam is a turning point in the dynamics along the CNN coordinate. This would account for the drop in photoisomerization efficiency when exciting $\pi\pi^*$ as compared to nπ^* excitation. Finally, 1.5 ps long MD simulations (performed for technical reasons at CASSCF level) reveal that intramolecular vibrational redistribution (IVR) from the bending and stretching modes into the torsional mode occurs on a 1 ps time scale (SI, Figure S17). Thus, we associate the experimental 2.8 ps lifetime to the decay of the remaining nπ^* population through the widely accepted torsional mechanism.

In conclusion, we have combined TA spectroscopy with sub-20 fs temporal resolution in the UV range with state-of-the-art computational tools to study the ultrafast photodynamics of *trans*-AB. We were able to resolve the lifetime of the $\pi\pi^*$ state, the buildup of the nπ^* population, and the subsequent coherent oscillatory dynamics. We observe a single ultrafast lifetime (~50 fs) of the $\pi\pi^*$ state, which is correlated to the buildup of the nπ^* ESA. Theoretical simulations reproduce with remarkable accuracy the positions of all ESA bands from the $\pi\pi^*$ and nπ^* states and reveal the origin of the ps-lasting oscillations of the intensity of the photoinduced absorption signals and, thus, the nature of the vibrational dynamics activated immediately after decay to the nπ^* state. Four "hot" modes, all characterized by strong symmetric in-plane bending deformations in the central CNNC fragment, were identified: 200 cm^{-1}, 300 cm^{-1}, 650 cm^{-1}, and 850 cm^{-1}. The observed intensity beat pattern is a signature of the localization of large amount of energy (10000 cm^{-1}) in these four modes during the first 1 ps, causing strong modulations of the absorption cross section. Radiative to kinetic energy transfer opens a non-radiative channel to the GS, inaccessible upon nπ^* excitation (Figure 4). The interplay between theory and experiment allows us to assign the so-called "CNN-bending" channel as the main reason behind the violation of the Kasha rule and behind the QY reduction at shorter wavelengths, *cis*-AB being formed only after IVR from the bending modes into the torsion on the ps time scale. Finally, neither the experimental nor the theoretical results call for additional ESs in order to describe the $\pi\pi^*$ depopulation dynamics: all experimental spectral features can be accurately reproduced using only the $\pi\pi^*$ and nπ^* states.

■ ASSOCIATED CONTENT

Supporting Information

Sample preparation, LA spectrum, experimental setup, results of the data analysis, simulation protocols for nonlinear spectroscopy and molecular dynamics, simulation parameters, simulated spectra, molecular orbitals and Cartesian coordinates. The following files are available free of charge. The Supporting Information is available free of charge on the ACS Publications website at DOI: 10.1021/acs.jpclett.8b00152.

(PDF)

■ AUTHOR INFORMATION

Corresponding Authors

*E-mail: giulio.cerullo@polimi.it.
*E-mail: marco.garavelli@unibo.it.

ORCID

Artur Nenov: 0000-0003-3071-5341
Javier Segarra-Martí: 0000-0002-2076-3406
Simone Taioli: 0000-0003-4010-8000
Shaul Mukamel: 0000-0002-6015-3135
Marco Garavelli: 0000-0002-0796-289X

Present Address

◆École Polytechnique Fédérale de Lausanne, CH-1015 Lausanne, Switzerland

Author Contributions

○These authors contributed equally.

Notes

The authors declare no competing financial interest.

■ ACKNOWLEDGMENTS

This work was supported by the European Research Council Advanced Grant STRATUS (ERC-2011-AdG No. 291198) to GC and MG. RBV is thankful for support from the European Commission through the Marie Curie actions (FP7-PEOPLE-IEF-2012). SM gratefully acknowledges the support of NSF, grant CHE 1663822.

■ REFERENCES

(1) Feringa, B. L.; Browne, W. R. *Molecular Switches*, 2nd ed.; Wiley-VCH Verlag GmbH & Co. KgaA: Weinheim, Germany, 2011.

(2) Ikeda, T.; Tsutsumi, O. Optical Switching and Image Storage by Means of Azobenzene Liquid-crystal Films. *Science* **1995**, *268*, 1873–1875.

(3) Renner, C.; Moroder, L. Azobenzene as Conformational Switch in Model Peptides. *ChemBioChem* **2006**, *7*, 868–878.

(4) Spörlein, S.; Carstens, H.; Satzger, H.; Renner, C.; Behrendt, R.; Moroder, L.; Tavan, P.; Zinth, W.; Wachtveitl, J. Ultrafast Spectroscopy Reveals Subnanosecond Peptide Conformational Dynamics and Validates Molecular Dynamics Simulation. *Proc. Natl. Acad. Sci. U. S. A.* **2002**, *99*, 7998–8002.

(5) Banghart, M. R.; Volgraf, M.; Trauner, D. Engineering Light-Gated Ion Channels. *Biochemistry* **2006**, *45*, 15129–15141.

(6) Mahimwalla, Z.; Yager, K. G.; Mamiya, J.; Shishido, A.; Priimagi, A.; Barrett, C. J. Azobenzene Photomechanics: Prospects and Potential Applications. *Polym. Bull.* **2012**, *69*, 967–1006.

(7) Munkerup, K.; Romanov, D.; Bohinski, T.; Stephansen, A. B.; Levis, R. J.; Sølling, T. I. Conserving Coherence and Storing Energy during Internal Conversion: Photoinduced Dynamics of cis-and trans-Azobenzene Radical Cations. *J. Phys. Chem. A* **2017**, *121*, 8642–8651.

(8) Rau, H.; Lueddecke, E. On the Rotation-Inversion Controversy on Photoisomerization of Azobenzenes. Experimental Proof of Inversion. *J. Am. Chem. Soc.* **1982**, *104*, 1616–1620.

(9) Rau, H. Photoisomerization of benzenes. In *Photoreactive Organic Thin Films*; Academic Press: Boston, 2002.

(10) Cho, J.; Berbil Bautista, L.; Levy, N.; Poulsen, D.; Fréchet, J. M. J.; Crommie, M. F. Functionalization, Self-assembly, and Photoswitching Quenching for Azobenzene Derivatives Adsorbed on Au (111). *J. Chem. Phys.* **2010**, *133*, 234707.

(11) Pechenezhskiy, I. V.; Cho, J.; Nguyen, G. D.; Berbil-Bautista, L.; Giles, B. L.; Poulsen, D. A.; Fréchet, J. M. J.; Crommie, M. F. Self-Assembly and Photomechanical Switching of an Azobenzene Derivative on GaAs (110): A Scanning Tunneling Microscopy Study. *J. Phys. Chem. C* **2012**, *116*, 1052–1055.

(12) Bandara, H. M. D.; Burdette, S. C. Photoisomerization in Different Classes of Azobenzene. *Chem. Soc. Rev.* **2012**, *41*, 1809–1825.

(13) Lednev, I. K.; Ye, T.; Hester, R. E.; Moore, J. N. Femtosecond Time-Resolved UV–Visible Absorption Spectroscopy of trans-Azobenzene in Solution. *J. Phys. Chem.* **1996**, *100*, 13338–13341.

(14) Lednev, I. K.; Ye, T.; Matousek, P.; Towrie, M.; Foggi, P.; Neuwahl, F. V. R.; Umapathy, S.; Hester, R. E.; Moore, J. N. Femtosecond Time-Resolved UV-Visible Absorption Spectroscopy of trans-Azobenzene: Dependence on Excitation Wavelength. *Chem. Phys. Lett.* **1998**, *290*, 68–74.

(15) Fujino, J.; Tahara, T. Picosecond Time-Resolved Raman Study of trans-Azobenzene. *J. Phys. Chem. A* **2000**, *104*, 4203–4210.

(16) Fujino, T.; Arzhantsev, S. Yu.; Tahara, T. Femtosecond Time-Resolved Fluorescence Study of Photoisomerization of trans-Azobenzene. *J. Phys. Chem. A* **2001**, *105*, 8123–8129.

(17) Fujino, T.; Arzhantsev, S. Yu.; Tahara, T. Femtosecond/Picosecond Time-Resolved Spectroscopy of trans- Azobenzene: Isomerization Mechanism Following $S_2(\pi\pi^*)\leftarrow S_0$ Photoexcitation. *Bull. Chem. Soc. Jpn.* **2002**, *75*, 1031–1040.

(18) Satzger, H.; Root, C.; Braun, M. Excited-State Dynamics of trans- and cis-Azobenzene after UV Excitation in the $\pi\pi^*$ Bband. *J. Phys. Chem. A* **2004**, *108*, 6265–6271.

(19) Naegele, T.; Hoche, R.; Zinth, W.; Wachtveitl, J. Femtosecond Photoisomerization of cis-Azobenzene. *Chem. Phys. Lett.* **1997**, *272*, 489–495.

(20) Satzger, H.; Spoerlein, S.; Root, C.; Wachtveitl, J.; Zinth, W.; Gilch, P. Fluorescence Spectra of trans-and cis-Azobenzene–Emission from the Franck–Condon State. *Chem. Phys. Lett.* **2003**, *372*, 216–223.

(21) Schultz, T.; Quenneville, J.; Levine, B.; Toniolo, A.; Martinez, T. J.; Lochbrunner, S.; Schmitt, M.; Shaffer, J. P.; Zgierski, M. Z.; Stolow, A. Mechanism and Dynamics of Azobenzene Photoisomerization. *J. Am. Chem. Soc.* **2003**, *125*, 8098–8099.

(22) Rau, H. Further Evidence for Rotation in the π,π^* and Inversion in the n,π^* Photoisomerization of Azobenzenes. *J. Photochem.* **1984**, *26*, 221–225.

(23) Stuart, C. M.; Frontiera, R. R.; Mathies, R. A. Excited-State Structure and Dynamics of cis- and trans-Azobenzene from Resonance Raman Intensity Analysis. *J. Phys. Chem. A* **2007**, *111*, 12072–12080.

(24) Kim, Y.; Phillips, J. A.; Liu, H.; Kang, H.; Tan, W. Using Photons to Manipulate Enzyme Inhibition by an Azobenzene-Modified Nucleic Acid Probe. *Proc. Natl. Acad. Sci. U. S. A.* **2009**, *106*, 6489–6494.

(25) Quick, M.; Dobryakov, A. L.; Gerecke, M.; Richter, C.; Berndt, F.; Ioffe, I. N.; Granovsky, A. A.; Mahrwald, R.; Ernsting, N. P.; Kovalenko, S. A. Photoisomerization Dynamics and Pathways of trans- and cis-Azobenzene in Solution from Broadband Femtosecond Spectroscopies and Calculations. *J. Phys. Chem. B* **2014**, *118*, 8756–8771.

(26) Monti, S.; Orlandi, G.; Palmieri, P. Features of the Photochemically Active State Surfaces of Azobenzene. *Chem. Phys.* **1982**, *71*, 87–99.

(27) Ishikawa, I.; Noro, T.; Shoda, T. Theoretical Study on the Photoisomerization of Azobenzene. *J. Chem. Phys.* **2001**, *115*, 7503–7512.

(28) Conti, I.; Garavelli, M.; Orlandi, G. The Different Photoisomerization Efficiency of Azobenzene in the Lowest $n\pi^*$ and $\pi\pi^*$

Singlets: the Role of a Phantom State. *J. Am. Chem. Soc.* **2008**, *130*, 5216−5230.

(29) Casellas, J.; Bearpark, M. J.; Reguero, M. Excited-State Decay in the Photoisomerisation of Azobenzene: A New Balance between Mechanisms. *ChemPhysChem* **2016**, *17*, 3068−3079.

(30) Harabuchi, Y.; Ishii, M.; Nakayama, A.; Noro, T.; Taketsugu, T. A Multireference Perturbation Study of the NN Stretching Frequency of trans-Azobenzene in $n\pi^*$ Excitation and an Implication for the Photoisomerization Mechanism. *J. Chem. Phys.* **2013**, *138*, 064305.

(31) Tan, E. M. M.; Amirjalayer, S.; Smolarek, S.; Vdovin, A.; Zerbetto, F.; Buma, W. J. Fast Photodynamics of Azobenzene Probed by Scanning Excited-State Potential Energy Surfaces Using Slow Spectroscopy. *Nat. Commun.* **2015**, *6*, 5860.

(32) Ootani, Y.; Satoh, K.; Nakayama, A.; Noro, T.; Taketsugu, T. Ab Initio Molecular Dynamics Simulation of Photoisomerization in Azobenzene in the $n\pi^*$ State. *J. Chem. Phys.* **2009**, *131*, 194306.

(33) Yuan, S.; Dou, Y.; Wu, W.; Hu, Y.; Zhao, J. Why Does trans-Azobenzene Have a Smaller Isomerization Yield for $\pi\pi^*$ Excitation than for $n\pi^*$ Excitation? *J. Phys. Chem. A* **2008**, *112*, 13326−13334.

(34) Tiberio, G.; Muccioli, L.; Berardi, R.; Zannoni, C. How Does the trans−cis Photoisomerization of Azobenzene Take Place in Organic Solvents? *ChemPhysChem* **2010**, *11*, 1018−1028.

(35) Cembran, A.; Bernardi, F.; Garavelli, M.; Gagliardi, L.; Orlandi, G. On the Mechanism of the cis-trans Isomerization in the Lowest Electronic States of Azobenzene: S_0, S_1, and T_1. *J. Am. Chem. Soc.* **2004**, *126*, 3234−3243.

(36) Altoe, P.; Bernardi, F.; Conti, I.; Garavelli, M.; Negri, F.; Orlandi, G. Light Driven Molecular Switches: Exploring and Tuning Their Photophysical and Photochemical Properties. *Theor. Chem. Acc.* **2007**, *117*, 1041−1059.

(37) Conti, I.; Marchioni, F.; Credi, A.; Orlandi, G.; Rosini, G.; Garavelli, M. Cyclohexenylphenyldiazene: a Simple Surrogate of the Azobenzene Photochromic Unit. *J. Am. Chem. Soc.* **2007**, *129*, 3198−3210.

(38) Böckmann, M.; Doltsinis, N. L.; Marx, D. Unraveling a Chemically Enhanced Photoswitch: Bridged Azobenzene. *Angew. Chem., Int. Ed.* **2010**, *49*, 3382−3384.

(39) Moreno, M.; Gelabert, R.; Lluch, J. M. The Quest for Photoswitches Activated by Near-Infrared Light. A Theoretical Study of the Photochemistry of BF_2-Coordinated Azo Derivatives. *ChemPhysChem* **2016**, *17*, 2824−2838.

(40) Borrego-Varillas, R.; Candeo, A.; Viola, D.; Garavelli, M.; De Silvestri, S.; Cerullo, G.; Manzoni, C. Microjoule-Level, Tunable Sub-10 fs UV Pulses by Broadband Sum-Frequency Generation. *Opt. Lett.* **2014**, *39*, 3849−3852.

(41) Borrego-Varillas, R.; Oriana, A.; Branchi, F.; De Silvestri, S.; Cerullo, G.; Manzoni, C. Optimized Ancillae Generation for Ultra-Broadband Two-Dimensional Spectral-Shearing Interferometry. *J. Opt. Soc. Am. B* **2015**, *32*, 1851−1855.

(42) Borrego-Varillas, R.; Oriana, A.; Ganzer, L.; Trifonov, A.; Buchvarov, I.; Manzoni, C.; Cerullo, G. Two-Dimensional Electronic Spectroscopy in the Ultraviolet by a Birefringent Delay Line. *Opt. Express* **2016**, *24*, 28491−28499.

(43) Mukamel, S. *Principles of Nonlinear Optical Spectroscopy*; Oxford University Press: New York, 1995.

(44) Mukamel, S.; Abramavicius, D. Many-Body Approaches for Simulating Coherent Nonlinear Spectroscopies of Electronic and Vibrational Excitons. *Chem. Rev.* **2004**, *104*, 2073−2098.

(45) Abramavicius, D.; Palmieri, B.; Voronine, D. V.; Sanda, F.; Mukamel, S. Coherent Multidimensional Optical Spectroscopy of Excitons in Molecular Aggregates; Quasiparticle versus Supermolecule Perspectives. *Chem. Rev.* **2009**, *109*, 2350−2408.

(46) Nenov, A.; Rivalta, I.; Mukamel, S.; Garavelli, M. Bidimensional Electronic Spectroscopy on Indole in Gas Phase and in Water from First Principles. *Comput. Theor. Chem.* **2014**, *1040-1041*, 295−303.

(47) Nenov, A.; Mukamel, S.; Garavelli, M.; Rivalta, I. Two-Dimensional Electronic Spectroscopy of Benzene, Phenol, and Their Dimer: an Efficient First-Principles Simulation Protocol. *J. Chem. Theory Comput.* **2015**, *11*, 3755−3771.

(48) Nenov, A.; Giussani, A.; Segarra-Martì, J.; Jaiswal, V. K.; Rivalta, I.; Cerullo, G.; Mukamel, S.; Garavelli, M. Modeling the High-Energy Electronic State Manifold of Adenine: Calibration for Nonlinear Electronic Spectroscopy. *J. Chem. Phys.* **2015**, *142*, 212443.

(49) van Stokkum, I. H. M.; Larsen, D. S.; van Grondelle, R. Global and Target Analysis of Time-Resolved Spectra. *Biochim. Biophys. Acta, Bioenerg.* **2004**, *1657*, 82−104.

(50) Snellenburg, J. J.; Laptenok, S. P.; Seger, R.; Mullen, K. M.; van Stokkum, I. H. M. Glotaran: A Java-Based Graphical User Interface for the R Package TIMP. *J. Stat. Software* **2012**, *49*, 1−22.

(51) Pepino, A. J.; Segarra-Martí, J.; Nenov, A.; Improta, R.; Garavelli, M. Resolving Ultrafast Photoinduced Deactivations in Water-Solvated Pyrimidine Nucleosides. *J. Phys. Chem. Lett.* **2017**, *8*, 1777−1783.

DOI: 10.1021/acs.jpclett.8b00152